Thermodynamic Behavior of Particle/Diblock Copolymer Mixtures: Simulation and Theory

June Huh, Valeriy V. Ginzburg, and Anna C. Balazs*

Department of Chemical and Petroleum Engineering, University of Pittsburgh, Pittsburgh, Pennsylvania 15261

Received April 21, 2000; Revised Manuscript Received August 2, 2000

ABSTRACT: We investigate the influence of hard nanoparticles on the phase behavior of diblock copolymers. Using Monte Carlo simulations, we obtain phase diagrams as a function of the nanoparticle size and concentration. When the size of the nanoparticles becomes comparable to the radius of gyration of the minority (A) block, we observe the formation of new superstructures, where the particles self-assemble inside the copolymer micelles. We develop a theoretical model, based on the strong segregation limit approximation, and show that these self-assembled structures can be either stable or metastable, depending on the particle size and volume fraction. The formation of such phases is due to the interplay between the particle−particle excluded-volume interactions, preferential particle/block-A interactions, and the enthalpic and stretching interactions within the diblock.

I. Introduction

The majority of high-performance polymers involve a blend of macromolecules and solid "filler" particles, which serve to improve the properties of the polymeric matrix. Recently, there has been significant interest in the development of composites where the polymeric matrix is composed of block copolymers. For example, a composite consisting of a diblock polyelectrolyte and carbon black nanoparticles was shown to exhibit improved electric conductivity and mechanical stability, making it an optimal material for solid-state rechargeable batteries.[1] As another example, mixing diblock copolymers with clay nanoparticles yields new polymer/clay nanocomposites with increased mechanical strength and toughness; in particular, adding only 5 wt % of clay to the copolymer increases the tensile modulus 1.4 times.[2] Block copolymers were also used as "templates" to control the deposition of metal particles onto thin films.[3,4] Such diblock/particle mixtures are now being synthesized for ultimate use in photonic band gap devices.[5]

While there have been a number of experimental studies on fabricating diblock/particle composites,[3−7] there have been few theoretical investigations into the factors that control the thermodynamic and kinetic behavior of these systems. In recent studies,[8−10] the structural evolution of symmetric diblocks in the presence of particles was modeled using mesoscopic techniques (dynamical density functional[8] and cell dynamical systems[9,10] theories). These simulations revealed how the local lamellar ordering is influenced by the particles and how the particles, in turn, self-assemble in the preferentially wetting blocks. These studies provide significant insight into the kinetic behavior of the mixture. Additional studies, however, are needed to determine the stability of the observed structures and map out equilibrium phase diagrams.

The difficulty in determining the phase behavior of copolymer/particle composites stems mainly from the presence of several length scales within the system: the monomer size, the particle size, and the radius of gyration of the polymer chain. In typical experiments, the nanoparticles are larger than the monomer units yet smaller than the radius of gyration of the chain.[3,7] In the majority of previous theoretical treatments of block copolymers systems (pure diblock copolymer melts,[11−14] diblock copolymer solutions, mixtures of two or more diblock copolymers, etc.), all the structures essentially consisted of the same-size monomer units.

In this paper, we use both Monte Carlo simulations and a simple theoretical model to study the phase behavior of the diblock copolymer/particle mixtures. Through the simulations, we determine the morphology of the mixtures and calculate density profiles and structure factors. On the basis of these results, one can determine approximate phase diagrams as a function of diblock composition and particle volume fraction. The topology of the phase diagram crucially depends on the particle size, and for large particles (when the particle size is comparable to the radius of gyration of the smaller block), new self-assembled structures are observed. To describe these structures, we develop a simple analytical theory based on a scaling model for diblocks in the strong segregation limit (SSL). Using this theory, we predict that large particles can indeed self-assemble within the minority block (to which they have a preferential attraction) and form structures resembling the core−shell morphologies in triblock copolymers[15,16] or cylindrical superstructures in diblock copolymer mixtures.[17] We conclude by analyzing the stability of these new structures.

II. Monte Carlo Simulations

A. Simulation Method. We study the behavior of a diblock copolymer/particle mixture using a dynamic canonical Monte Carlo simulation model. The simulation box is $40 \times 40 \times 40$ cubic lattice sites in size, with periodic boundary conditions along the x, y, and z directions. Into this box, we introduce cubic particles with linear size R and volume $V = R^3$ and diblock copolymer chains $A_{Nf}B_{N(1-f)}$, where $N = 32$ monomers and the composition f is varied in the range $0 < f < 0.5$. In addition to varying f, we alter the particle volume fraction, ϕ. To facilitate the motion of the polymers and particles, a fraction of void sites, $\phi_v = 0.3$, are also introduced into the box.

10.1021/ma000708y CCC: $19.00
Published on Web 09/29/2000

The polymer chains and particles obey excluded-volume constraints. (Each lattice site can only be occupied by a particle or a monomer or be a void site.) Apart from the excluded-volume interaction, we introduce enthalpic interactions between the nearest neighbors. We let ϵ_{AB} represent the interaction energy between the A- and B-monomers and ϵ_{PB} represent the particle−B-monomer interaction. Here, $\epsilon_{AB} = \epsilon_{PB} = \epsilon > 0$, and all other interaction parameters are set to zero. Thus, the particles have an affinity toward the A-block.

We update the conformations of the polymer chains using the "slithering snake" algorithm[18] and allow the particles to change their positions by migrating to nearest-neighboring voids. The configurational space is sampled according to the Metropolis algorithm.[19] The initial configuration is prepared by equilibrating the system under athermal conditions (which corresponds to the high-temperature limit). Starting from this athermal state, we then lower the temperature in small steps of $\Delta(N\epsilon/k_BT) = 0.1$. At every step, we use the equilibrated configuration from the previous temperature as a starting point for the new one. For each value of $(N\epsilon/k_BT)$, the system is allowed to equilibrate for a time exceeding its relaxation time, τ. We determine τ by measuring the decay of the autocorrelation function of a chosen observable (e.g., the number of contacts between particles). After equilibration, we calculate the properties of the system by performing thermodynamic averaging over 100 independent runs by using the sub-block averaging method.[20]

B. Simulation Results. In this section, we present the simulation results for mixtures containing small ($R = 1$) and large ($R = 3$) particles. Our main aim is to determine the phase behavior and structures of these copolymer/particle mixtures for various diblock compositions f and particle volume fractions ϕ within the strong segregation limit.

To determine the phase behavior of the system, we must "calibrate" our simulations by relating the segmental interaction parameter, $\epsilon' = \epsilon/k_BT$, to the effective Flory−Huggins parameter, χ. (Recall that we take the particles to be chemically identical to the A-block, so there is just one effective Flory−Huggins parameter in the problem.) To carry out this calibration, we perform a simulation of a pure diblock copolymer melt. To express χ as a function of ϵ', we numerically calculate the structure factor $S(k)$, defined by

$$S(\mathbf{k}) = L^{-3}\langle \sum_{u,v} e^{i\mathbf{k}(\mathbf{r}_u - \mathbf{r}_v)} \psi(\mathbf{r}_u)\, \psi(\mathbf{r}_v)\rangle \tag{1}$$

$$S(k) = \frac{\sum_{|\mathbf{k}|=k} S(\mathbf{k})}{\sum_{|\mathbf{k}|=k} 1} \tag{2}$$

where the $\mathbf{r}_i$ are the coordinates of site i in the simulation box and the order parameter ψ is defined as the deviation of the A-monomer concentration from the average value, $\psi(\mathbf{r}) = \phi_A(\mathbf{r}) - f$. The bracket indicates a thermodynamic average over different configurations. Equation 2 defines the spherically averaged scattering function, $S(k)$. It was shown[11] that for the pure diblock copolymer melt $S(k)$ is given by

$$S(k)^{-1} = \Gamma(k) - 2\chi \tag{3}$$

where $\Gamma(k)$ is related to the Fourier transforms of the *intrachain* monomer density correlation functions (assuming Gaussian statistics) and χ is the Flory interaction parameter. The Flory parameter χ is related to ϵ' in the following manner:

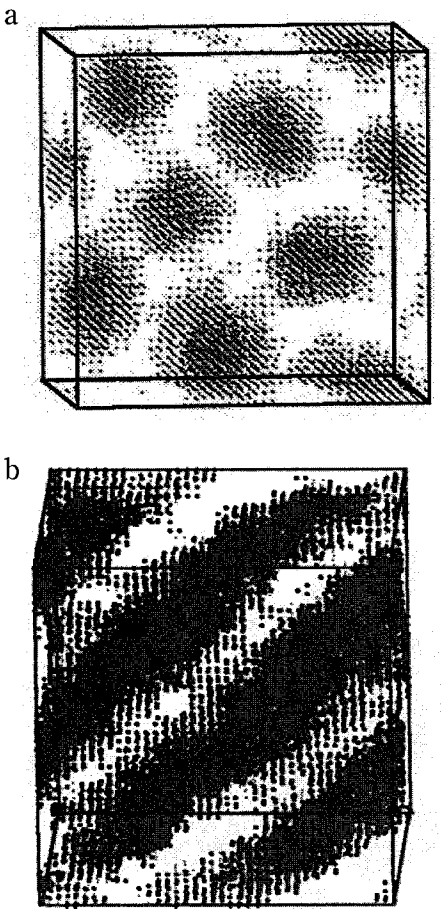

Figure 1. Snapshots of the simulation box for $f = 0.25$, $N\chi \approx 50$, $\phi = 0$ (a), and $\phi = 0.5$ (b). Particle size $R = 1$. Gray dots represent A-block, white space corresponds to the B-block, and black dots are particles.

$$\chi = z_{eff}\epsilon' \tag{4}$$

where z_{eff} is the effective coordination number. The value of z_{eff} in eq 4 is thus given by the slope in the plot of $S(k)^{-1}$ vs ϵ'. We find $z_{eff} \approx 1.8$. By analyzing the scattering factor for different values of ϵ', we find that the order−disorder transition (ODT) occurs at $N\epsilon' \approx 10$ ($N\chi \approx 18$). Note that this value of ODT is different from the mean-field result of $N\chi \approx 10.5$.[11] Such a discrepancy is a result of the finite chain length ($N = 32$) and the presence of the voids. In the following, we fix the value of $N\chi \approx 50$, which is in the strong segregation regime for the pure diblock copolymer, and add the particles.

Small Particles ($R = 1$). In Figure 1, we present snapshots of the simulation box for the diblock composition $f = 0.25$. Figure 1a shows the melt without particles, and Figure 1b shows the mixture with $\phi = 0.5$ (50 vol %) of added small particles. By comparing the two figures, it can be seen that particles modifiy the structure from the cylindrical (C) to the lamellar (L) phase as they disperse within the A regions. The particles appear to be randomly distributed within the A phase, and no macroscopic phase separation between particles and block copolymers takes place.

To characterize the spatial distribution of particles relative to the A-blocks, it is convenient to calculate the concentration correlation between the A-monomers and

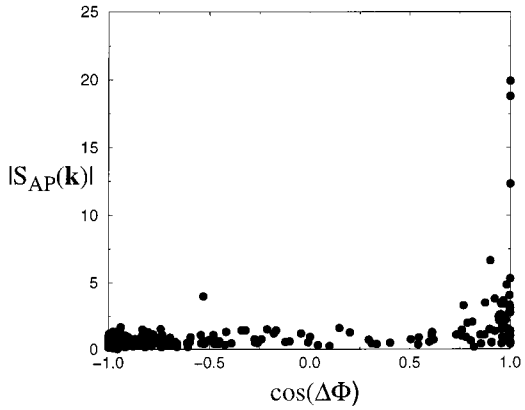

Figure 2. Scatter plot of $|S_{AP}(\mathbf{k})|$ vs the phase difference cos(ΔΦ) for the system $f = 0.25$, $N\chi \approx 50$, and $\phi = 0.5$. The dominant structure (largest magnitude of $|S_{AP}(\mathbf{k})|$) occurs for cos(ΔΦ) = 1, indicating that the particles and the A-monomers are "in phase" (particles randomly disperse within A-block).

the particles:

$$S_{A,P}(\mathbf{k}) = L^{-3}\langle \sum_{u,v} e^{i\mathbf{k}(\mathbf{r_u}-\mathbf{r_v})} \psi_A(\mathbf{r_u})\, \psi_P(\mathbf{r_v})\rangle \qquad (5)$$

where the subscripts A and P stand for A-monomers and particles, respectively. The order parameters, ψ_i (i = A, P), are given by $\psi_A(\mathbf{r}) = \phi_A(\mathbf{r}) - f(1 - \phi)(1 - \phi_v)$ and $\psi_P(\mathbf{r}) = \phi_P(\mathbf{r}) - \phi(1 - \phi_v)$. From eq 5, we can determine the phase difference, ΔΦ, between the concentration profiles of A-monomers and particles as[21]

$$\cos(\Delta\Phi) = \frac{\mathrm{Re}(S_{A,P}(\mathbf{k}))}{|S_{A,P}(\mathbf{k})|} \qquad (6)$$

where Re denotes the real part of the complex number $S_{A,P}(\mathbf{k})$, and $|S_{AP}(\mathbf{k})|$ is its absolute value. We calculate both cos(ΔΦ) and $|S_{AP}(\mathbf{k})|$ for wavevectors in the range $0 < k < 1.5$ (corresponding to wavelengths λ_x, λ_y, and λ_z that vary between $L/4$ and L) and plot these values in the manner shown in Figure 2. We can see that the largest value of $|S_{AP}(\mathbf{k})|$ is found at ΔΦ = 0, which implies that the profile of the A-monomers is "in phase" with the profile of the particles. This result suggests that the particles are not segregated from the block copolymer but are dispersed randomly within the A-block in the microphase-separated structure.[22]

From the simulations, we construct an approximate phase diagram for diblock copolymer/small particle mixtures as plotted in Figure 3. Here, the interaction parameter is $N\chi \approx 50$, and the phase structures are denoted as L (lamellar), C (cylindrical), S (spherical), and D (disordered). The diblock composition f is varied within $0 < f < 0.5$ (minority A); the particle volume fraction ϕ is varied between 0 and 0.5. On the phase diagram, the position of each letter represents a simulation point in (f−ϕ) space. The phase structures are determined from the graphical output of the simulations and the scattering functions. We observe that all of the phase-separated structures are microscopically ordered phases (no macrophase separation occurs). The particles modify the structure of ordered phases compared to the no-particle system. This phase diagram agrees qualitatively with recent theoretical calculations for the phase behavior of diblock copolymers with selective solvents,[23] which presumably act much like small particles.

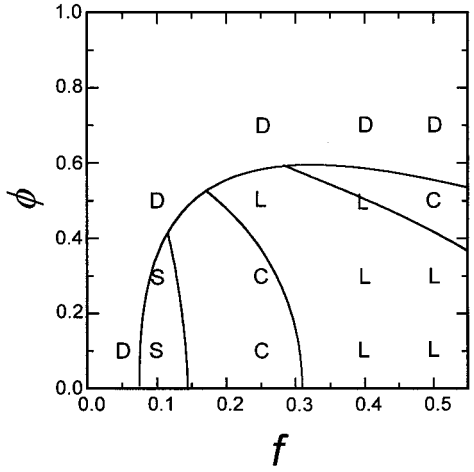

Figure 3. Approximate phase diagram for the copolymer/particle mixture in the $N\chi \approx 50$, $R = 1$ case. Letters correspond to simulated points, while lines serve as guide to eye. Phases: D = disordered, L = lamellar, C = cylindrical, S = spherical.

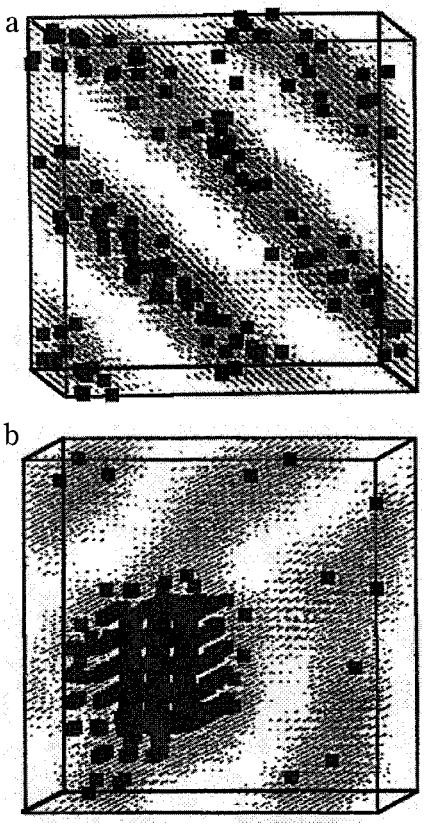

Figure 4. Snapshots of the simulation box for $f = 0.5$, $N\chi \approx 50$, $\phi = 0.1$ (a), and $\phi = 0.2$ (b). Particle size $R = 3$.

Large Particles (R = 3). We now consider the case where the particles are comparable to the radius of gyration of the A-block. Figure 4 shows snapshots of the system for $f = 0.5$, $N\chi \approx 50$, and $R = 3$. In Figure 4a, $\phi = 0.1$, and in Figure 4b, $\phi = 0.2$. For the lower particle volume fraction in (a), one can see the lamellar phase, with the particles being randomly dispersed within the A-lamellae. As the particle volume fraction is increased (see Figure 4b), the particles segregate from the diblocks and the system exhibits two-phase coexistence (between the macroscopically phase-separated particles and the lamellar phase).

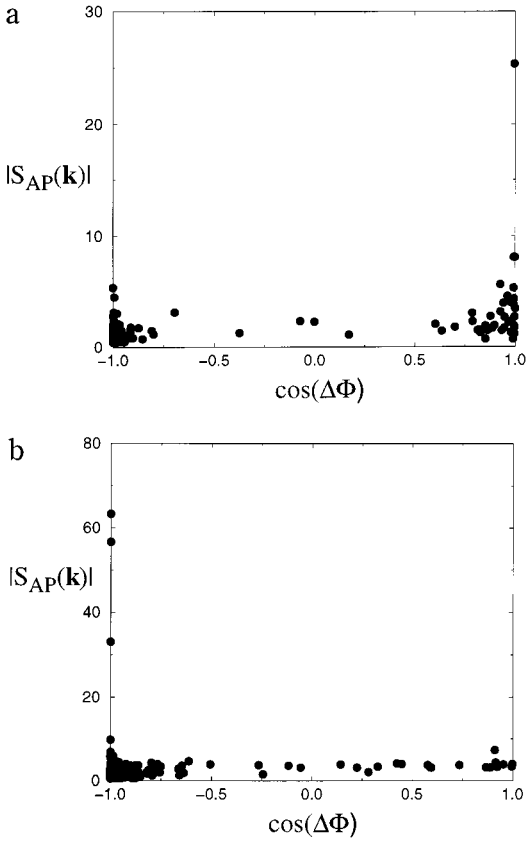

Figure 5. Scatter plot of $|S_{AP}(\mathbf{k})|$ vs the phase difference cos(ΔΦ) for the system $f = 0.5$, $N\chi \approx 50$, $\phi = 0.1$ (a), and $\phi = 0.2$ (b). Particle size $R = 3$.

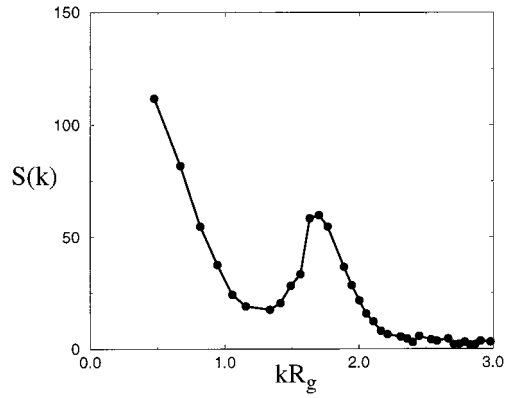

Figure 6. Spherically averaged scattering factor, S, vs the dimensionless wavenumber, kR_g, for the system $f = 0.5$, $\phi = 0.2$. Particle size $R = 3$.

To describe the spatial distribution of the particles relative to the A-block, we calculate the phase difference between the particles and A-monomers (see Figure 5). For the mixture with 10% particles (Figure 4a), the dominant fluctuation is found when $\Delta\Phi = 0$, indicating that the particles are indeed randomly dispersed within the A-lamellae. For the mixture with 20% particles (Figure 4b), the phase difference for the dominant fluctuation is 180°, so that the particles are separated from the diblock. To confirm that the system is macrophase-separated, we calculate the spherically averaged structure factor $S(k)$, as shown in Figure 6. The calculation shows that the structure factor is a decreasing function of k for small values of k (up to $kR_g \approx 1.4$), where R_g is the radius of gyration of a copolymer chain (measured for this specific f and χ). The peak that appears at $kR_g \approx 1.8$ is due to the ordering of the pure block copolymer. Since the function $S(k)$ is decreasing for small k, we conclude that either the system is macroscopically phase-separated or the length scale of its ordering is larger than the size of the simulation box. (Note that because of the finite size of our lattice, we cannot probe fluctuations with wavelengths $\lambda \geq L$.)

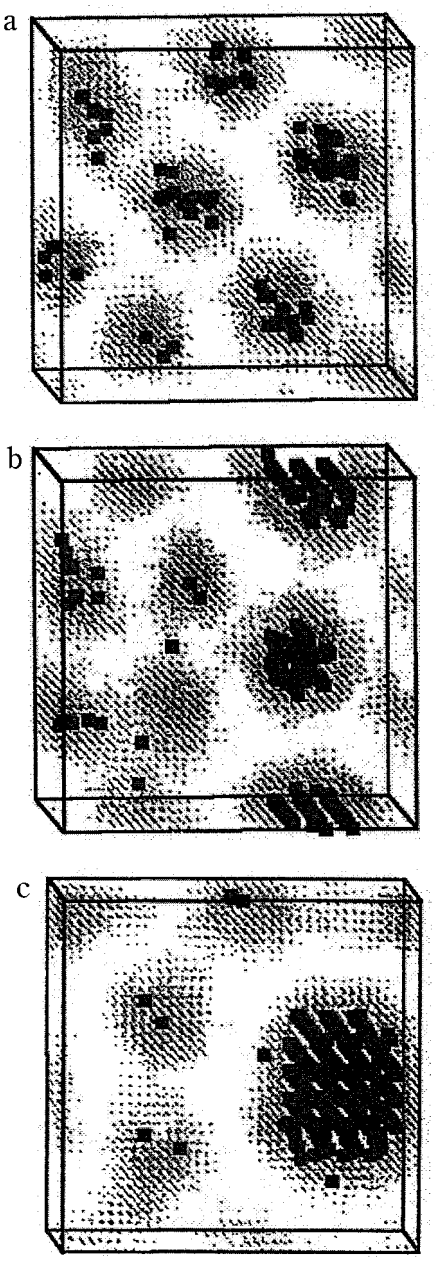

Figure 7. Snapshots of the simulation box for $f = 0.25$, $N\chi \approx 50$, $\phi = 0.05$ (a), $\phi = 0.10$ (b), and $\phi = 0.15$ (c). Particle size $R = 3$.

We now study the effect of changing the diblock composition f. When f is decreased, the length of the A-block becomes smaller, and the chains have to stretch more to accommodate the particles. Thus, one can expect that for smaller f, the particles and the polymers would become less compatible. Figure 7 shows snapshots of the system for $f = 0.25$, $N\chi \approx 50$, $R = 3$, and the following three values of ϕ: (a) $\phi = 0.05$, (b) $\phi = 0.10$, and (c) $\phi = 0.15$. The images confirm our expectation concerning the effects of decreasing f. For $\phi = 0.05$ (see Figure 7a), the mixture is in the cylindrical phase, with the particles randomly dispersed within the A-cylinders. For $\phi = 0.15$

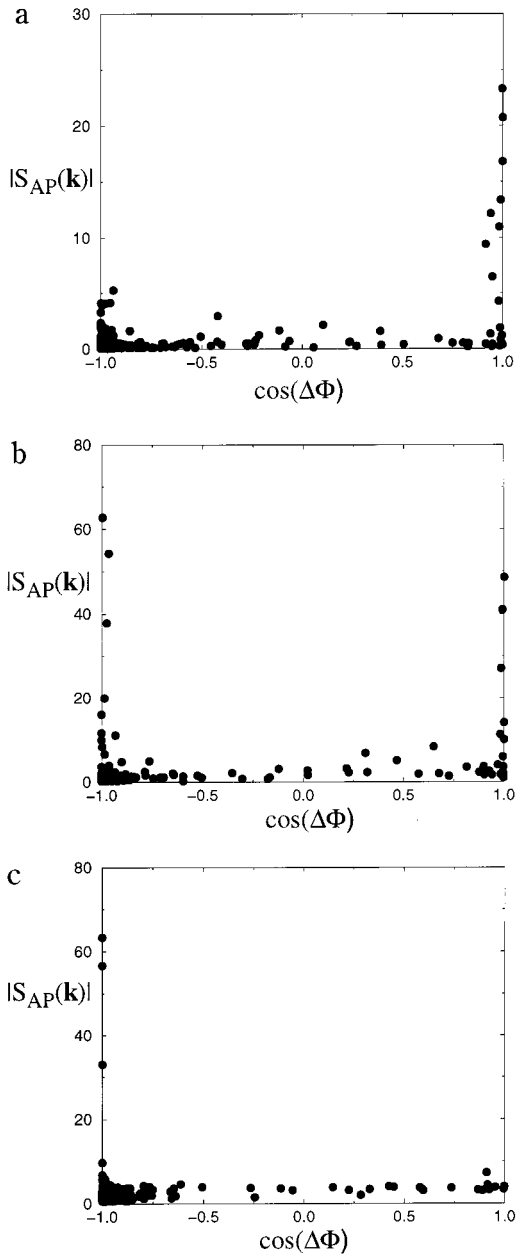

Figure 8. Scatter plot of $|S_{AP}(\mathbf{k})|$ vs the phase difference cos(ΔΦ) for the system $f = 0.25$, $N\chi \approx 50$, $\phi = 0.05$ (a), $\phi = 0.10$ (b), and $\phi = 0.15$ (c). Particle size $R = 3$.

(Figure 7c), the system exhibits a clear two-phase coexistence between the particles and the diblocks. The intermediate case, $\phi = 0.1$ (Figure 7b), shows the apparent two-phase coexistence between the pure diblock and some "mixed" phase in which particles and diblocks are microphase-separated. In this phase, the particles self-assemble into a "core" cylinder, surrounded by a "shell" consisting of the A-block. From the calculation of the phase difference between A and P (Figure 8), we see that the particles are "in phase" with the A-block for $\phi = 0.05$ and "out of phase" for $\phi = 0.1$ and $\phi = 0.15$, in agreement with observed morphologies.

To better understand the nature of the new structure seen for the case $\phi = 0.1$, we repeated our simulations for the same particle volume fraction but slightly increased the length of the A-block ($f = 0.3125$). This increase in f makes it easier for the chains to accommodate the particles and should stabilize the microphase ordered structures. Indeed, the snapshot of the

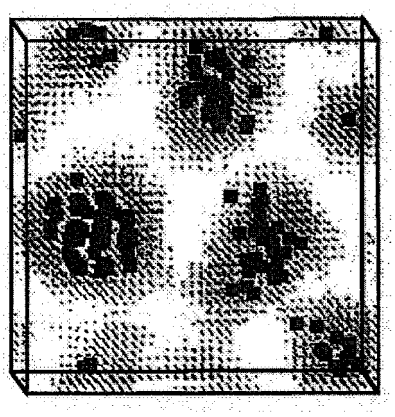

Figure 9. Snapshot of the simulation box for $f = 0.3125$, $N\chi \approx 50$, and $\phi = 0.1$. Particle size $R = 3$.

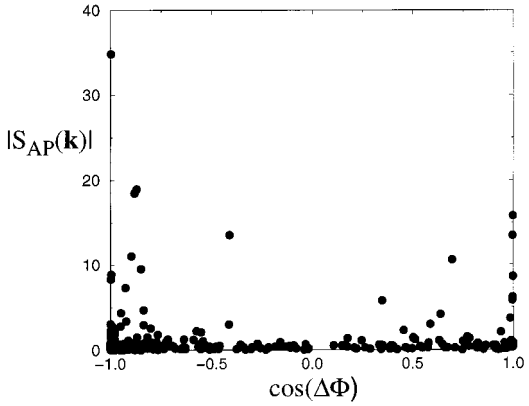

Figure 10. Scatter plot of $|S_{AP}(\mathbf{k})|$ vs the phase difference cos(ΔΦ) for the system $f = 0.3125$, $N\chi \approx 50$, and $\phi = 0.1$. Particle size $R = 3$.

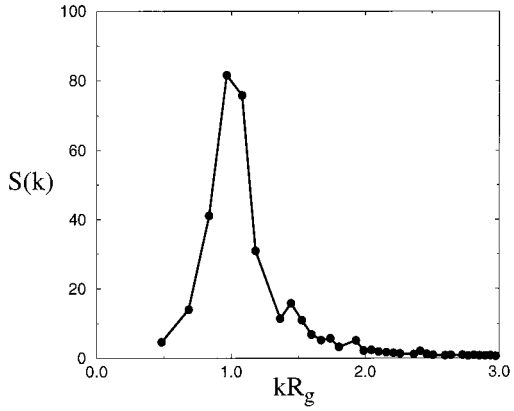

Figure 11. Spherically averaged scattering factor, S, vs the dimensionless wavenumber, kR_g, for the system $f = 0.3125$ and $\phi = 0.1$. Particle size $R = 3$.

system (Figure 9) shows the new "core−shell" cylindrical morphology. The phase difference between A and P is 180° (Figure 10), indicating that the particles are segregated from the A-block (as well as from the B-block). However, the calculation of the spherically averaged scattering factor (Figure 11) shows that there is no macrophase separation; the system clearly exhibits a microscopically ordered structure.

We can combine our results for different values of f and ϕ and sketch an approximate phase diagram, as shown in Figure 12. As in Figure 3, the position of each letter represents the simulation point. The simulations are performed primarily for $\phi < 0.2$ since the particles

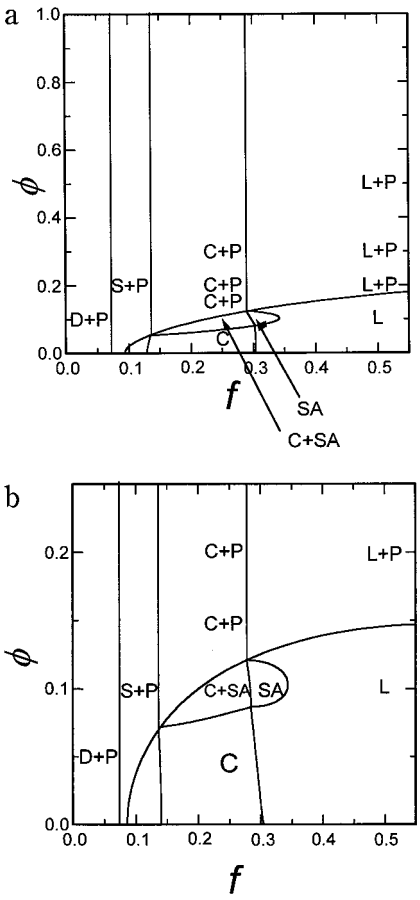

Figure 12. Approximate phase diagram for the copolymer/particle mixture in the $N\chi \approx 50$, $R = 3$ case (a), and enlargement of the small-ϕ region (b). Letters correspond to simulated points, while lines serve as guide to eye. Phases: D = disordered, L = lamellar, C = cylindrical, S = spherical, SA = "self-assembled" core−shell structures.

are strongly segregated from the block copolymers for $\phi > 0.2$ so that the structures are already in the region of two-phase coexistence. Our investigation is focused on determining the boundary between the "in-phase" and "out-of-phase" structures. When ϕ is small and f is not too small, the particles disperse in the A-block. As ϕ is increased and/or f is decreased, the A-chains can no longer accommodate the particles; the particles become segregated from both A- and B-blocks. This results, in most cases, in macrophase separation between the pure diblock and the particle-rich phase. We find, however, that in a narrow region of diblock compositions and particle volume fractions this segregation can lead to the formation of new *microscopically* ordered phases. In such phases (denoted SA on the phase diagram), one observes a self-assembly of both particles and diblocks into one superstructure. To better understand the origins of such behavior, we propose the following theoretical model.

III. Theory

A. Free Energy and Mesophases. To develop a theoretical description for the phase behavior of the mixture, we employ the strong segregation limit (SSL) approximation, first formulated by Semenov.[12] Within this approach (which is typically valid in the low-temperature limit, $\chi N \gg 10$), it is assumed that the melt of diblocks is divided into pure-A and pure-B regions, separated by narrow interfacial areas. Because of the incompressibility of the mixture, the A-blocks and B-blocks are highly stretched. The balance between the stretching free energy of the blocks and the energy of the AB-interfaces determines the equilibrium morphology of the mixture as a function of the diblock composition, f, and the particle volume fraction, ϕ. For simplicity, we will restrict ourselves to the three "classical" diblock structures (lamellar, cylindrical, and spherical) and neglect the bicontinuous phases[13,24−26] that exist only in a very narrow composition range. We will, however, take into account the disordered phase, since, as we saw from the simulations, the addition of particles promotes a order−disorder transition at large ϕ.

While it may seem paradoxical to integrate the strong segregation model with a study of the disordered phase, this approach was successfuly applied by Floudas et al.[27] to study the phase behavior of copolymer/homopolymer mixtures. Floudas et al. found that the transition temperatures calculated using this combined approach differ from exact values by less than 10%. In the following, we will write down the free energies of the ordered and disordered phases and calculate the equilibrium states and the phase diagrams.

Ordered Phases. We assume that the system can adopt one of the following structures (see Figure 13): lamellar (a), cylindrical (b or c), or spherical (d or e). As in the simulations, we assume that $\chi_{AP} = 0$, $\chi_{BP} = \chi_{AB} = \chi$. Because of the selective interaction, the particles are restricted to the area occupied by the A-block. However, we also conjecture that the particles are not necessarily dispersed in a uniform manner within the A-region. To characterize the particle distribution over the A-blocks, we introduce a new variable ψ, which is the "apparent" particle volume fraction. It is easy to see that, for a given diblock composition, f, and particle volume fraction, ϕ, the "apparent" volume fraction ψ must lie between ϕ/f_{eff}, where $f_{eff} = \phi + f(1 - \phi)$, and 1. When $\psi = \phi/f_{eff}$, the particles are dispersed uniformly over the entire A-region. On the other hand, when $\psi = 1$, the particles are completely separated from the A-block within the micelle.

The free energy density contribution due to the particles can be written as

$$g_{part} \approx n_p\left[\log(\psi) + \Psi_{CS}(\psi) + (1-\psi)\frac{R_p^2}{4Nfa_0^2}\right] = \frac{\phi}{v_p}\left[\log(\psi) + \Psi_{CS}(\psi) + (1-\psi)\frac{R_p^2}{4Nfa_0^2}\right] \quad (7)$$

where R_p and $v_p = {}^4/_3\pi R_p^3$ are the particle radius and volume, respectively, and $a_0 = 1/\sqrt{6}$. The first and second term in the right-hand side (rhs) represent the ideal and nonideal parts of the translational entropy of the hard-sphere gas with the packing fraction of spheres equal to ψ. The nonideal part is approximated by the Carnahan−Starling[28] equation:[29]

$$\Psi_{CS}(\psi) = \frac{4\psi - 3\psi^2}{(1-\psi)^2} \quad (8)$$

The third term in the rhs of eq 7 describes the effective "depletion interaction" between the particles and the polymer. The particles dispersed in a polymer brush acquire effective "surface tension" since the area occupied by a particle is blocked for the nearby polymer

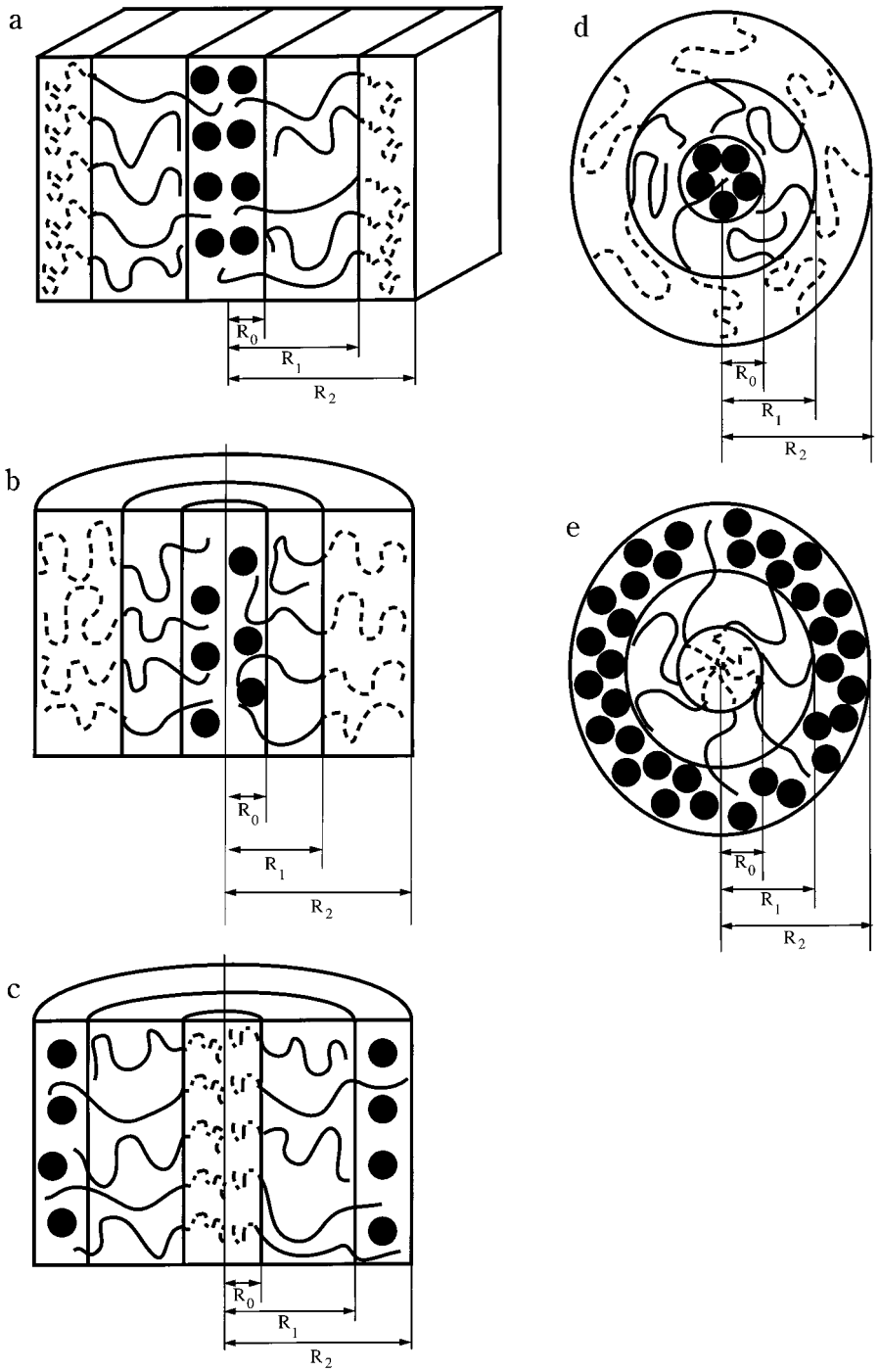

Figure 13. Schematic representation of ordered mesophases: lamellar (a); cylindrical, majority-B (b); cylindrical, majority-A (c); spherical, majority-B (d); spherical, majority-A (e). In all cases, three possible regions are shown: B-region, A-rich region, and particle-rich region (in which some A-chains are also present). Solid wavy lines depict A-blocks, dashed wavy lines represent B-blocks, and circles correspond to particles.

chains. This interaction has been calculated for several specific cases of particles in brushes.[30−32] Here, we use the following simple scaling estimate for this term. Each A-subchain incurs an additional free energy loss due to the stretching in the "transverse" direction (to get around the particles):

$$h_{tr} \simeq \frac{nR_p^2}{4a_0^2Nf} \tag{9}$$

where n is the number of particles per chain. In the limit of small ϕ (and ψ), we can estimate n as

$$n \sim \frac{\phi}{v_p}\frac{N}{1-\phi} \tag{10}$$

As ψ is increased, the number of particle−polymer contacts begins to drop, since more particles become segregated from the polymer chains. Thus, n is reduced by roughly a factor of $1 - \psi$. By combining eqs 9 and 10 and multiplying by the additional factor $1 - \psi$, we get the third term in the rhs of eq 7.

We now consider other terms in the free energy. As shown by Semenov,[12] the free energy of the polymer chains can be divided into an elastic part, g_{el}, and a surface part, g_{surf}, given by the respective equations:

$$g_{el} = \kappa \frac{R_2^2}{N^2 a_0^2} \quad (11)$$

$$g_{surf} = \lambda \chi^{1/2} \frac{a_0}{R_2} \quad (12)$$

The prefactors κ and λ depend on the specific morphology (lamellar, cylindrical, or spherical), the nature of the majority phase (A or B), the particle volume fraction ϕ, the diblock composition f, and the "apparent" particle volume fraction ψ. The parameter R_2 is the size of the Wigner−Seitz cell. We derive expressions for κ and λ in Appendices A and B. Finally, we add the mixing (translational) free energy for the diblock copolymer chains, which is given as

$$g_{mix} = \frac{1-\phi}{N} \log(1-\phi) \quad (13)$$

By combining eqs 11−13 and minimizing them with respect to the micelle radius (size of the Wigner−Seitz cell) R_2, we obtain the final expression for the free energy density:

$$g_{ord} \approx \frac{\phi}{v_p}\left[\log(\psi) + \Psi_{CS}(\psi) + (1-\psi)\frac{R_p^2}{4Nfa_0^2}\right] + \frac{1-\phi}{N}\log(1-\phi) + 3\chi^{1/3}(2N)^{-2/3}\lambda^{2/3}\kappa^{1/3} \quad (14)$$

To calculate the phase diagram, we minimize the rhs of eq 14 with respect to ψ for each ϕ and f and for each possible structure. The result of such minimization gives us the map of the lowest-energy ordered phases. To complete the phase diagram, we must compare these free energies with that of the disordered phase.

Disordered Phase. In the disordered phase, both particles and diblocks are dispersed uniformly in space. Thus, the particle-related free energy contribution (eq 7) can be modified to yield

$$g_{part} \approx \frac{\phi}{v_p}\left[\log(\phi) + \Psi_{CS}(\phi) + (1-\phi)\frac{R_p^2}{4Na_0^2}\right] \quad (15)$$

Here, we replace ψ with ϕ and Nf with N due to the fact that now the particles are not confined to the A-regions. The monomer−monomer and monomer−particle short-range interactions yield another contribution that can be estimated as

$$g_{ent} = \chi(1-\phi)(1-f)[f(1-\phi) + (\phi/v_p)\Sigma_p] = \chi(1-f_{eff})[f(1-\phi) + \phi(0.5/R_p)] \quad (16)$$

The parameter Σ_p is the number of "surface contacts" for each particle, so the density of unfavorable BP contacts depends on the surface-to-volume ratio for the particles. We normalize the ratio so that for $R_p = 0.5$ the expression coincides with the one derived for the diblock in a solvent (with particles playing the role of solvent molecules). The total free energy density of a disordered phase is given by (again, we add the mixing entropy of the diblocks, eq 13)

$$g_{dis} = \frac{\phi}{v_p}\left[\log(\phi) + \Psi_{CS}(\phi) + (1-\phi)\frac{R_p^2}{4Na_0^2}\right] + \frac{1-\phi}{N} \times \log(1-\phi) + \chi(1-f_{eff})[f(1-\phi) + \phi(0.5/R_p)] \quad (17)$$

We can now calculate the phase behavior of the system as a function of the particle size, R_p. These phase diagrams are discussed in the next subsection.

B. Phase Diagrams. We consider three systems with different particle radii: (a) $R_p = 1.0$, (b) $R_p = 2.0$, and (c) $R_p = 4.0$. The polymer chain length, N, and the Flory parameter, χ, are kept constant: $N = 50$, $\chi = 1.0$. The approximate phase diagrams are shown in Figures 14−16. It can clearly be seen that the size of the nanoparticles plays an important role in determining phase behavior of the final composite. This strong dependence on particle size is also evident from the simulations. As we point out below, similar trends are seen in copolymer/homopolymers mixtures when the degree of polymerization of the homopolymer is increased.

When R_p is small compared to the radius of gyration of the A-block, the particles are uniformly dispersed in the A-rich regions (if the system is in one of the ordered phases) or in the entire mixture (if the system is in the disordered state). For this case, the phase behavior of the diblock/particle mixture is similar to that of the diblock in a selective solvent.[23,33] Indeed, one can see that the phase diagram plotted in Figure 14 is qualitatively similar to the ones calculated by Huang and Lodge.[23]

By comparing the phase diagram shown in Figure 14 with the phase diagram for the pure diblock melt,[12] we can conclude the following. First, adding small nanoparticles to the diblock strongly reduces the order−disorder transition temperature.[34] Second, for a given temperature and diblock composition, adding particles with preferential attraction to one of the blocks causes changes in the system morphology (for example, from lamellar to cylindrical for $f = 0.65$). These results are also in a qualitative agreement with the simulations and the theoretical studies of adding relatively short homopolymers to copolymer/homopolymer mixtures.[27,35−37]

When the particle size is slightly increased (Figure 15), the coexistence regions become broader, and the order−disorder transition moves toward higher ϕ. The larger particles are less effective in decreasing the order−disorder transition than the small ones. This result also agrees with observations in copolymer/homopolymer mixtures when the homopolymers' degree of polymerization is increased.[27]

We now turn to the more interesting case in which the particle radius becomes comparable to the radius of gyration of the A-block, at least in some (relatively broad) range of compositions. In Figure 16, we plot the approximate phase diagram for the case $R_p = 4$. This phase diagram is markedly different from the previous ones in several respects. First, all coexistence regions become noticeably broad (unlike the earlier cases where the transition between the ordered phases showed almost no biphasic regions). Second, for most of the systems where the A-block is in the minority ($f < 0.5$), the mixture phase-separates into the pure diblock and the particle-rich phase. (Note that because of the packing constraints, described by the Carnahan−Starling term in the free energy, one cannot obtain a pure particle phase; the fraction of polymer in the particle-rich phase is still about 30%.) Finally, the

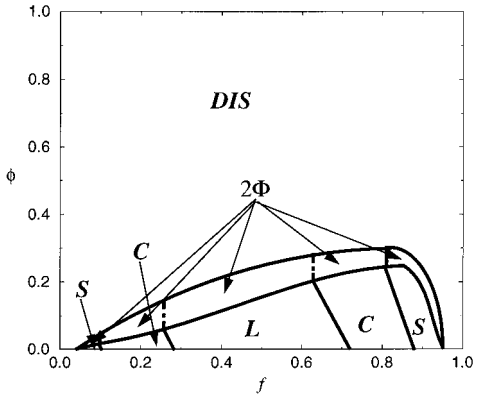

Figure 14. Phase diagram of the diblock/particle mixture. Particle radius $R_p = 1$. Phases: DIS = disordered, S = spherical, C = cylindrical, L = lamellar, 2Φ = two-phase regions.

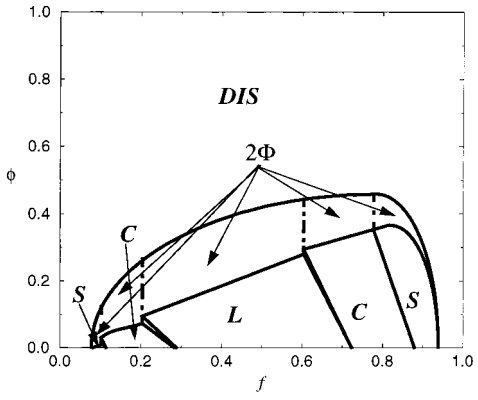

Figure 15. Same as in Figure 14, but with $R_p = 2$.

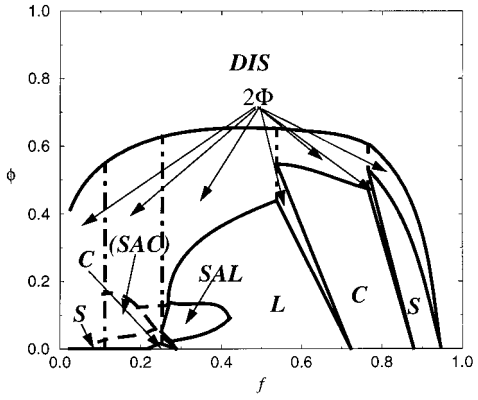

Figure 16. Same as in Figure 14, but with $R_p = 4$. Note the appearance of new mesophases: SAL = self-assembled lamellar and SAC = self-assembled cylindrical. SAC phase is always metastable, while SAL can be both stable and metastable.

system can exhibit interesting new morphologies: self-assembled lamellar (SAL) and self-assembled cylindrical (SAC) phases, in which some of the particles form a "condensate" *within* the underlying microphase-separated structure of the diblock. We note the agreement between the theory and the simulation results in the previous section on the location of the SA phases. Since the SA structure is an "exclusive" characteristic of diblock/particle mixtures (it is not observed in copolymer solutions or copolymer/homopolymer mixtures[38]), we will discuss it in more detail.

Because of the large particle size, it is unfavorable for the particles to disperse in the A-block (the inner block of the spherical, cylndrical, or lamellar micelle). Therefore, some fraction of the particles begins to "precipitate" and form a smaller, particle-rich inner block inside the A + P region. This additional microsegregation decreases the elastic energy of the A-chains while keeping the energy of the B-block unchanged. The penalty for this, however, is the increase in the particle-related free energy term due to the loss of translational entropy (both ideal and nonideal contributions). The balancing of the two contributions leads to the phase transitions and the formation of equilibrium spherical, cylindrical, and lamellar superstructures with three layers: (i) the inner, particle-rich region; (ii) the central, A-rich region; and (iii) the outer, B-block region. We call these phases self-assembled (SA) structures (SAS, SAC, and SAL) to distinguish them from the classical S, C, and L structures where only two regions (A-rich and B-rich) exist in each micelle. In SA-phases, particles "self-assemble" into spheres, tubes, or sheets surrounded by the A-chains.

Because of the precarious balance of forces creating the SA-phases, in most cases these phases are unstable or metastable with respect to the macrophase separation between the particle-rich phase and the pure diblock. Such macrophase separation would decrease the elastic energy of the copolymer chains. However, due to the compatibility between the particles and A-blocks, the particles increase the effective composition of the A species, and thus, the mixed system has a more symmetric composition than the pure diblock melt. Furthermore, unlike polymer or solvent, particles cannot form "pure" phases (because of the excluded-volume constraint), so even a macrophase-separated particle-rich phase still contains a significant amount of polymer needed to fill the voids. Both of these factors make microphase separation more favorable than macrophase separation. The interplay between these effects determines which morphology becomes stable.

We see that new superstructures can exist only in a narrow region of diblock compositions (for $R_p = 4$, it is roughly $0.2 < f < 0.4$). The phase behavior is extremely sensitive to particle radius, particle volume fraction, and diblock composition. To illustrate this point, we plot the free energy density, g, as a function of the particle volume fraction, ϕ, for two diblock compositions (Figure 17). For the composition $f = 0.21$ (Figure 17a), the mixture undergoes the following sequence of phase transitions (where the numbers refer to the values of ϕ at the transition points): C−0.05−SAC−0.12−L−0.37−DIS. Both SAC and L phases are metastable within the broad two-phase coexistence between the pure diblock and the particle-rich disordered phase. When we plot g vs ϕ for the composition $f = 0.31$ (Figure 17b), a similar sequence L−0.05−SAL−0.12−L−0.47−DIS can be observed without the broad macrophase separation. All phases (including the SAL) appear to be stable at least in some narrow range of particle volume fractions. Thus, it is possible to achieve thermodynamically stable mixtures with SA-structures, although these would occupy very narrow regions on the phase diagram. The majority of SA-phases would be metastable or even unstable, and the mixture would eventually macrophase-separate into pure polymer and particle-rich phases. We note, however, such metastable phases could be long-lived or become kinetically trapped and thus could readily be experimentally observed.

If the particle size is increased even further, "complete immiscibility" between the diblocks and the particles

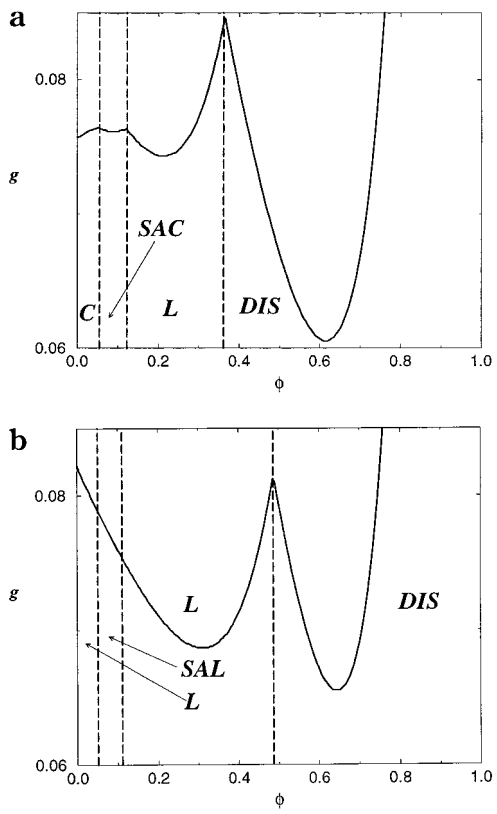

Figure 17. Free energy density, g, as a function of the particle volume fraction, ϕ: diblock composition $f = 0.21$ (a); diblock composition $f = 0.31$ (b).

would be observed for almost all diblock compositions. The phase diagram would then reduce to one broad two-phase region between the ordered diblocks and the disordered particle-rich phase, with one or more metastable SA-phases within this two-phase area. This behavior is, again, similar to that of copolymer/homopolymer mixtures in which the size of homopolymer molecules is much larger than that of the diblocks.[27,39]

IV. Conclusions

We studied the thermodynamic behavior of mixtures of diblock copolymers and hard spherical particles using Monte Carlo simulations and a scaling theory in the strong segregation limit (SSL). The particles interact with each other via excluded-volume steric effects and have a preferential attraction toward one of the components of the diblock. By varying the particle size and concentration, one can modify the morphology of the resulting mixture and either induce macroscopic phase separation between the particle-rich and diblock-rich phases or create potentially new microphase-separated structures.

From simulations and theoretical arguments, we conclude that, when the particle size is comparable to the radius of gyration of the minority block and the particles have a strong preferential attraction to this block, a new microphase ordering takes place in a narrow range of particle volume fractions and diblock compositions. The new ordered phases are made of three-layer micelles, with each micelle consisting of the following: (i) a particle-rich inner layer, (ii) an A-block central layer, and (iii) a B-block outer layer. In our simulations, we observe such a structure for the cylindrical phase; we also predict the existence of similar lamellar and spherical structures. Even though our SSL-based theory is semiqualitative and does not take into account many factors (such as multiparticle correlations or fluctuations due to finite chain length), we point to good agreement between the theory and simulations on the location of the SA phases. Namely, both methods indicate the existence of these SA structures at roughly the same narrow range of diblock compositions.

It is interesting to note that some elements of particle ordering within lamellar diblocks were observed by Hamdoun et al.[7] and by Morkved et al.[3,4] for particles whose radius was comparable to the lamellar thickness. Hamdoun et al. even observed the transition between the "dispersed" structure (when particles are uniformly dispersed within the A-lamellae) and the "segregated" structure (when particles self-assemble in the center of the A-lamellae). This transition is somewhat similar to the L−SAL transition described in our model. At the same time, the differences between the two cases (in the experiments, the mixture was a two-dimensional diblock film that was deposited on a substrate) prevent direct comparisons.

Elucidation of all the exact conditions for the particle self-assembly requires more elaborate studies taking into account many additional features. Our recent simulations on the phase separation in binary fluids with hard-rod colloidal particles[40] have shown that the shape of the particles strongly influences the phase behavior: anisotropic particles "corraled" into a minority phase are more prone to self-assembly than spherical particles (due to the onset of orientational ordering). In addition, phase behavior can be sensitive to the particle−particle long-range interactions (for example, dipole−dipole interaction). We plan to study the influence of these factors on the phase behavior of diblock/particle systems by combining a density functional theory approach for the particles with the strong segregation limit theory for the diblocks (similar to the method used in describing the phase behavior of polymer/clay composites[41,42]). These studies are currently underway.

Acknowledgment. This work was supported by the NSF, through Grant DMR0709101, DOE, through Grant DE-FG02-90ER-45438, and ONR, through Grant N00014-91-J-1363. We thank Drs. Dmitri Kuznetsov, Ekaterina Zhulina, Russell Thompson, and Alexei Likhtman for fruitful discussions.

Appendix A: Elastic Energy of Copolymer Micelles

The elastic free energy of a pure diblock copolymer in a strong segregated regime was first calculated by Semenov.[12] If we restrict ourselves to lamellar ($d = 1$), cylindrical ($d = 2$), and spherical ($d = 3$) phases, the stretching energy of the polymer chains is given by

$$U_{el} = U_{in} + U_{out} \tag{A1}$$

Both "inner" (U_{in}) and "outer" (U_{out}) contributions to the stretching free energy depend on the micelle dimensionality d. The expressions derived by Semenov are

$$U_{in}(1) = \frac{\pi^2}{96}(Q/a_0)^2 R_1 \tag{A2}$$

$$U_{in}(2) = \frac{\pi}{96}(Q/a_0)^2 \tag{A3}$$

$$U_{in}(3) = \frac{3\pi}{640}(Q/a_0)^2 R_1^{-1} \quad \text{(A4)}$$

$$U_{out}(1) = \frac{\pi^2}{96}(Q/a_0)^2(R_2 - R_1) \quad \text{(A5)}$$

$$U_{out}(2) = \frac{Q^2}{16\pi a_0^2} 2\ln(R_2/R_1) \quad \text{(A6)}$$

$$U_{out}(3) = \frac{Q^2}{16\pi a_0^2}\left(\frac{1}{R_1} - \frac{1}{R_2}\right) \quad \text{(A7)}$$

where R_1 and R_2 are the inner and outer radii of the outer brush, respectively; Q is the number of chains in the d-dimensional micelle. The relationship between Q and R's is determined from incompressibility constraints.

When particles are introduced in the system, the (A + P) region can be divided into particle-rich and particle-poor zones, depending on the value of the parameter ψ. In the limits $\psi = \phi/f_{eff}$ (particles are dispersed uniformly) and $\psi = 1$ (all particles microsegregate and create a new A−P interface), we can write down the elastic energies analytically; for all the intermediate values of ψ, we simply use linear interpolation between the two limits. The resulting expression for the elastic free energy density, $g_{el} = U_{el}/(c_d R_2^d)$ (where $c_d = 2, \pi, {}^4/_3\pi$ for $d = 1$, 2, and 3, respectively), is given by eq 11, with the prefactor κ having the following form:

lamellar phase:

$$\kappa(f,\phi,\psi) = (\pi/48)(1-\phi)^2(1 - q\phi) \quad \text{(A8)}$$

cylindrical phase, majority-B:

$$\kappa(f,\phi,\psi) = \frac{1}{16}(1-\phi)^2(-\log(f_{eff}) + q\log(f_{eff}/\phi) + p\pi^2/6) \quad \text{(A9)}$$

cylindrical phase, majority-A:

$$\kappa(f,\phi,\psi) = \frac{1}{16}(1-\phi)^2(-p\log(1-f_{eff}) - q\log(1-f) + \pi^2/6) \quad \text{(A10)}$$

spherical phase, majority-B:

$$\kappa(f,\phi,\psi) = \frac{1}{12}(1-\phi)^2((f_{eff}^{-1/3} - 1) + q(\phi^{-1/3} - f_{eff}^{-1/3}) + p(3\pi^2/40)f_{eff}^{-1/3}) \quad \text{(A11)}$$

spherical phase, majority-A:

$$\kappa(f,\phi,\psi) = \frac{1}{12}(1-\phi)^2[p((1-f_{eff})^{-1/3} - 1) + q(1 - f_{eff})^{-1/3} - (1-\phi)^{-1/3} + (3\pi^2/40)(1-f_{eff})^{-1/3}] \quad \text{(A12)}$$

where $f_{eff} = \phi + f(1-\phi)$, $q = (\psi - \psi_{min})/(1 - \psi_{min})$, $p = 1 - q$, and $\psi_{min} = \phi/f_{eff}$.

Appendix B: Surface Energy of Copolymer Micelles

The density of the surface free energy for the d-dimensional micelle is given by eq 12. The coefficient λ depends on d and f_{eff} as follows (we use expressions derived by Semenov[12] for the pure diblock melt, and replace f with f_{eff}):

lamellar phase:

$$\lambda = 1 \quad \text{(B1)}$$

cylindrical phase, majority-B:

$$\lambda = 2f_{eff}^{1/2} \quad \text{(B2)}$$

cylindrical phase, majority-A:

$$\lambda = 2(1 - f_{eff})^{1/2} \quad \text{(B3)}$$

spherical phase, majority-B:

$$\lambda = 3f_{eff}^{2/3} \quad \text{(B4)}$$

spherical phase, majority-A:

$$\lambda = 3(1 - f_{eff})^{2/3} \quad \text{(B5)}$$

References and Notes

(1) Soo, P. P.; Huang, B. Y.; Jang, Y. I.; Chiang, Y. M.; Sadoway, D. R.; Mayes, A. M. *J. Electrochem. Soc.* **1999**, *146*, 32.
(2) Hasegawa, N.; Okamoto, H.; Kawasumi, M.; Usuki, A. *J. Appl. Polym. Sci.* **1999**, *74*, 3359.
(3) Morkved, T. L.; Wiltzius, P.; Jaeger, H. M.; Grier, D. G.; Witten, T. A. *Appl. Phys. Lett.* **1994**, *64*, 422.
(4) Lin, B. H.; Morkved, T. L.; Meron, M.; Huang, Z. Q.; Viccaro, P. J.; Jaeger, H. M.; Williams, S. M.; Schlossman, M. L. *J. Appl. Phys.* **1999**, *85*, 3180. Zehner, R. W.; Lopes, W. A.; Morkved, T. L.; Jaeger, H.; Sita, L. R. *Langmuir* **1998**, *14*, 241.
(5) Fink, Y.; Urbas, A. M.; Bawendi, M. G.; Joannopoulos, J. D.; Thomas, E. L. *J. Lightwave Technol.* **1999**, *17*, 1963.
(6) Cole, D. H.; Shull, K. R.; Baldo, P.; Rehn, L. *Macromolecules* **1999**, *32*, 771.
(7) Hamdoun, B.; Ausserre, D.; Cabuil, V.; Joly, S. *J. Phys. II* **1996**, *6*, 493; **1996**, *6*, 503; **1996**, *6*, 1207. Lauter-Pasiuk, V.; Lauter, H. J.; Ausserre, D.; Gallot, Y.; Cabuil, V.; Hamdoun, B.; Kornilov, E. I. *Physica B* **1998**, *241−243*, 1092.
(8) Sevink, G. J. A.; Zvelindovsky, A. V.; van Vlimmeren, B. A. C.; Maurits, N. M.; Fraaije, J. G. E. M. *J. Chem. Phys.* **1999**, *110*, 2250.
(9) Balazs, A. C.; Ginzburg, V. V.; Qiu, F.; Peng, G.; Jasnow, D. *J. Phys. Chem. B* **2000**, *104*, 3411.
(10) Ginzburg, V. V.; Gibbons, C.; Qiu, F.; Peng, G.; Balazs, A. C. *Macromolecules* **2000**, *33*, 6140.
(11) Leibler, L. *Macromolecules* **1980**, *13*, 1602.
(12) Semenov, A. N. *Sov. Phys. JETP* **1985**, *61*, 733.
(13) Matsen, M. W.; Schick, M. *Phys. Rev. Lett.* **1994**, *72*, 2660.
(14) Matsen, M. W.; Schick, M. *Macromolecules* **1994**, *27*, 6761; **1994**, *27*, 7157.
(15) Zheng, W.; Wang, Z.-G. *Macromolecules* **1995**, *28*, 7215.
(16) Lyatskaya, Y. V.; Birshtein, T. M. *Polymer* **1995**, *36*, 975.
(17) Birshtein, T. M.; Lyatskaya, Y. V.; Zhulina, E. B. *Polymer* **1992**, *33*, 343.
(18) Wall, F. T.; Mandel, F. *J. Chem. Phys.* **1975**, *63*, 4592.
(19) Metropolis, N.; Rosenbluth, A. W.; Rosenbluth, M. N.; Teller, A. N.; Teller, E. *J. Chem. Phys.* **1953**, *21*, 1087.
(20) Straatsma, T. P.; Berendsen, H. J. C.; Stam, A. J. *Mol. Phys.* **1986**, *57*, 89.
(21) Huh, J.; Angerman, H.; ten Brinke, G. *Macromolecules* **1996**, *29*, 6328.
(22) Strictly speaking, this statement is applicable only if the system is in the strong segregation regime (which is the case in our study), so there are no B-blocks in the (A + P)-region. In this case, any local increase in the particle density would cause a corresponding decrease in the local density of A-block, and the two would be "out of phase". Conversely, the absence of "out of phase" modes indicates the random (uniform on average) distribution of particles within the (A + P)-region.
(23) Huang, C.-I.; Lodge, T. P. *Macromolecules* **1998**, *31*, 3556.
(24) Hajduk, D. A.; Harper, P. E.; Gruner, S. M.; Honeker, C. C.; Kim, G.; Thomas, E. L.; Fetters, L. J. *Macromolecules* **1994**, *27*, 4075.
(25) Olmsted, P. D.; Milner, S. T. *Phys. Rev. Lett.* **1994**, *72*, 936.

(26) Xi, H.; Milner, S. T. *Macromolecules* **1996**, *29*, 2404.
(27) Floudas, G.; Hadjichristidis, N.; Stamm, M.; Likhtman, A. E.; Semenov, A. N. *J. Chem. Phys.* **1997**, *106*, 3318.
(28) Carnahan, N. F.; Starling, K. E. *J. Chem. Phys.* **1969**, *51*, 635.
(29) We disregard the possibility of particle crystallization at high volume fractions. In principle, such an effect could affect the phase behavior of the composite. The role of crystallization will be considered in future studies.
(30) Solis, F. J.; Tang, H. *Macromolecules* **1996**, *29*, 7953.
(31) Subramanian, G.; Williams, D. R. M.; Pincus, P. A. *Macromolecules* **1996**, *29*, 4045.
(32) Witten, T. *Macromol. Rep.* **1992**, *A29*, 87.
(33) Birshtein, T. M.; Zhulina, E. B. *Polymer* **1990**, *31*, 1312.
(34) We did not study the dependence of $(N\chi)_{ODT}$ on ϕ systematically, having restrticted ourselves to the case of fixed temperature, $N\chi \approx 50$. However, the fact that particles promote disorder can be easily seen by noticing that the ODT occurs at $N\chi \approx 50$ for $f = 0.5$, $\phi \approx 0.2$, while the same transition for the no-particle case occurs at $N\chi \approx 10.5$.
(35) Likhtman, A. E.; Semenov, A. N. *Macromolecules* **1997**, *30*, 7273.
(36) Janert, P. K.; Schick, M. *Macromolecules* **1998**, *31*, 1109.
(37) We assume a uniform distribution of particles in the A-block. This approximation overstates the elastic (stretching) energy of the polymer chains. As a result, the order−disorder transitions are depressed toward lower values of ϕ, but the overall topology of the phase diagrams is not affected. Taking into account the inhomogeneous (parabolic) particle distribution is beyond the accuracy of this scaling approach, but will be the subject of future studies.
(38) When the homopolymer molecular weight is larger than that of the corresponding block in the copolymer, the homopolymer can form aggregates that exist within the underlying ordered structure of the diblock.[39] However, these structures are either metastable or even unstable but dynamically "frozen" states. The equilibrium state is still the macrophase-separated one.
(39) Pan, T.; Huang, K. L.; Balazs, A. C.; Kunz, M. S.; Mayes, A. M.; Russell, T. P. *Macromolecules* **1993**, *26*, 2860.
(40) Peng, G.; Qiu, F.; Ginzburg, V. V.; Jasnow, D.; Balazs, A. C. *Science* **2000**, *288*, 1802.
(41) Ginzburg, V. V.; Balazs, A. C. *Macromolecules* **1999**, *32*, 5681.
(42) Ginzburg, V. V.; Singh, C.; Balazs, A. C. *Macromolecules* **2000**, *33*, 1089.

MA000708Y